Supporting Information

for

Heavy Atom Cluster Chains with Strong Spin-Orbit Coupling and Magnetic Cations in $Mn[PtBi_6I_{12}]$

Maria A. Herz,[†#] Julia-Maria Hübner,[†] Jörg Sichelschmidt,[§] Rico Friedrich,[†$] and Michael Ruck*[†§‡]

[†]Faculty of Chemistry and Food Chemistry, TUD Dresden University of Technology, 01062 Dresden, Germany

[#]Department of Quantum Matter Physics, École de Physique, University of Geneva, 24 Quai Ernest-Ansermet, 1211 Geneva 4, Switzerland

[§]Max Planck Institute for Chemical Physics of Solids, 01187 Dresden, Germany

[$]Helmholtz-Zentrum Dresden-Rossendorf, 01328 Dresden, Germany

[‡]Würzburg–Dresden Cluster of Excellence ct.qmat, TUD Dresden University of Technology, 01062 Dresden, Germany

Corresponding author's email address: michael.ruck@tu-dresden.de

Table of Contents

Introduction	S2
Thermal Analysis and Synthesis	S3
Scanning Electron Microscopy and Energy-Dispersive X-Ray Spectroscopy	S4
X-ray Diffraction	S5
Electrical Resistance Measurement	S6
Magnetic Measurements	S7
Heat Capacity	S7

Introduction

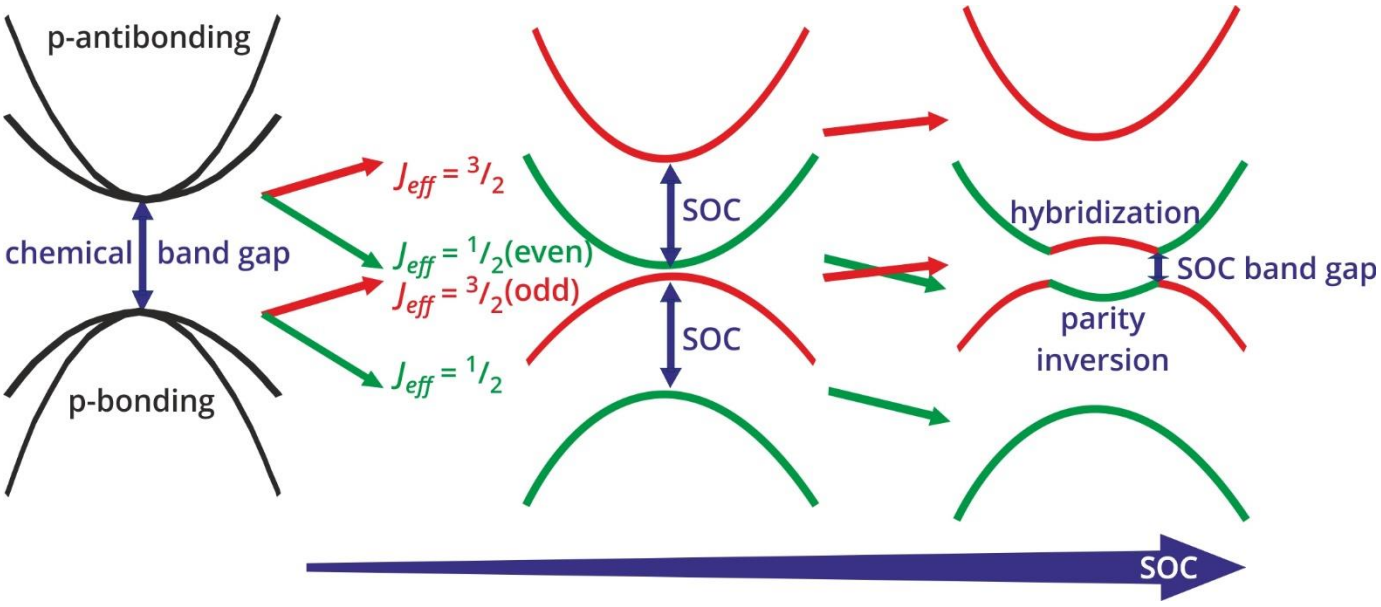

Figure S1. Schematic representation of the evolution of electronic bands created by p-states close to the Fermi level under the influence of increasing spin-orbit coupling (SOC). If SOC is large compared to the chemical band gap, an inversion of the band sequence and thus of the parity can occur, which results in a topologically non-trivial band gap.

Thermal Analysis and Synthesis

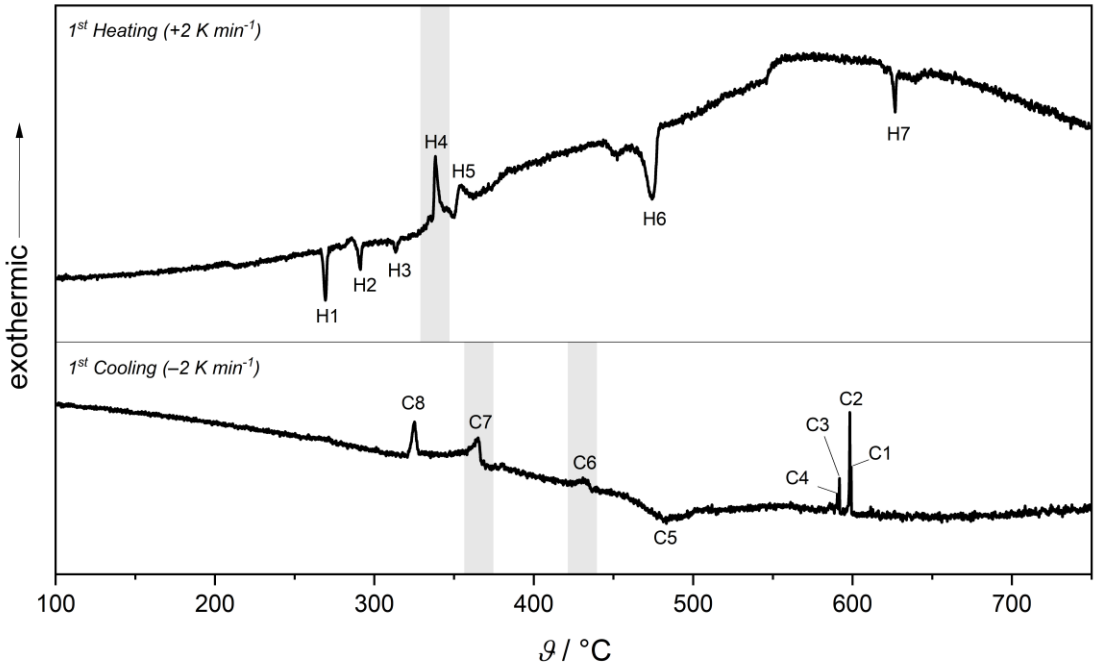

Figure S2. DSC data of a mixture with the molar ratio Mn : Pt : Bi : BiI_3 = 1 : 1 : 2 : 4. No signals could be observed below 100 °C and above 750 °C. The temperature intervals in which $(Bi_{2x}Mn_{1-3x})[PtBi_6I_{12}]$ formed are highlighted in grey. The effects in the heating and cooling curves are labelled and explained in Table S1.

Table S1. Allocation of DSC signals occurring during the heating to and cooling from 800 °C of a mixture with the molar ratio Mn : Pt : Bi : BiI_3 = 1 : 1 : 2 : 4 (see Figure S2). Compositions in parentheses refer to EDX analyses and seem to represent yet unknown compounds.

Signal	ϑ_{onset} / °C	ϑ_{peak} / °C	Effect	Allocation
H1	266	269	endothermic	melting of Bi
H2	281	285/291	endo- & exothermic	formation and decomposition of Bi_4I_4
H3	311	313	endothermic	formation of "$Bi_2Mn_2I_9$"
H4	336	338	exothermic	formation of $(Bi_{2x}Mn_{1-3x})[PtBi_6I_{12}]$ with $x \approx 0$
H5	345	349/353	endo- & exothermic	partial recrystallization of $(Bi_{2x}Mn_{1-3x})[PtBi_6I_{12}]$ with $x \approx 0$ under formation of $x \leq 0.16$ (probably entropy driven)
H6	445	452/473	endothermic	decomposition of $x \approx 0$, followed by decomposition of phases with higher x
H7	623	626	endothermic	decomposition of MnI_2
C1	599	599	exothermic	formation of "$BiMn_3I_7$" and "$Bi_2Mn_6I_7$"
C2	598	598	exothermic	formation of "$BiMn_2I_6$"
C3	592	591	exothermic	transformation to "Bi-doped MnI_2" and "$Bi_{13}Pt_5I_7$"
C4	590	590	exothermic	increased formation of MnI_2
C5	502	483	endothermic	decomposition of remaining ternary phases to BiI_3 and Bi_7I_2 and elements
C6	436	432	exothermic	formation of $(Bi_{2x}Mn_{1-3x})[PtBi_6I_{12}]$ with $x \leq 0.16$
C7	367	365	exothermic	partial recrystallization to $x \approx 0$
C8	327	325	exothermic	partial recrystallization to $Bi_2[PtBi_6I_{12}]_3$

Scanning Electron Microscopy and Energy-Dispersive X-Ray Spectroscopy

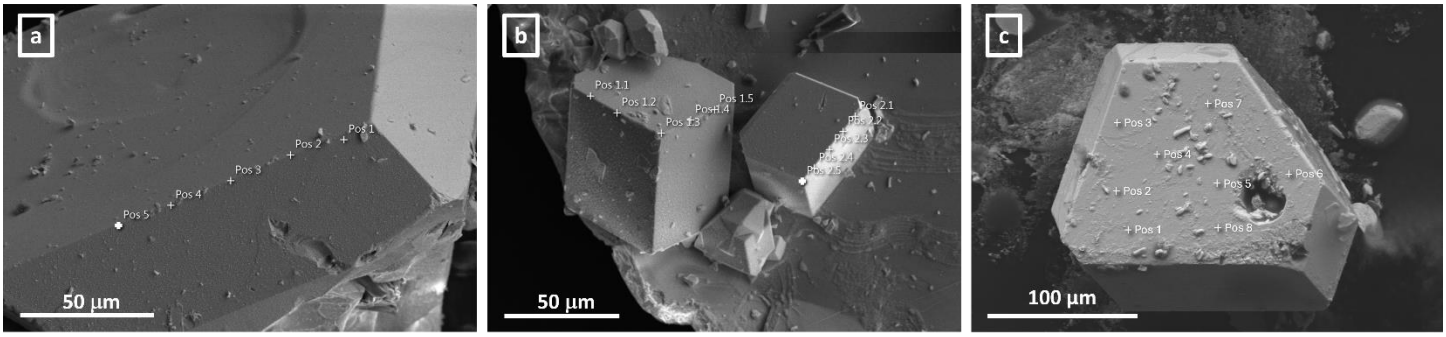

Figure S3. Scanning electron microscopic image of representative $Mn[PtBi_6I_{12}]$ crystals (a-c). Numbered locations marked by circles refer to EDX measurements shown in Table S2.

Table S2. Representative EDX analyses of $Mn[PtBi_6I_{12}]$ crystals obtained from a mixture of 1.33 : 1 : 2 : 4 of Mn : Pt : Bi : BiI_3 starting materials by the optimized synthesis protocol for single crystals. For location of points selected for measurements, see Figure S2. Expected composition for $Mn[PtBi_6I_{12}]$ (at.-%): Mn = 5, Pt = 5, Bi = 30, I = 60. The estimated accuracy of the shown measurements is 0.5 to 1 at.-%. The compositions of the samples were derived from such multiple EDX analyses by averaging.

Spectrum Label	Measured Elemental Compositions / at.-%			
Figure S2.a.	Mn	Pt	Bi	I
Pos 1	4.96	4.39	30.17	60.49
Pos 2	4.27	4.69	30.89	60.15
Pos 3	4.95	4.64	31.01	59.40
Pos 4	4.46	4.75	31.01	59.77
Pos 5	4.44	4.26	30.77	60.53
Figure S2.b.				
Pos 1.1	4.70	5.33	32.04	57.94
Pos 1.2	4.71	5.35	31.99	67.95
Pos 1.3	4.60	5.00	31.54	58.87
Pos 1.4	4.75	5.21	31.51	58.53
Pos 1.5	5.22	5.20	31.46	58.13
Pos 2.1	4.27	4.75	31.75	59.24
Pos 2.2	4.57	4.86	31.84	58.73
Pos 2.3	4.99	4.76	31.19	59.07
Pos 2.4	4.52	4.90	31.16	59.41
Pos 2.5	4.31	5.02	31.26	59.42
Figure S2.c				
Pos 1	3.65	4.98	32.05	59.32
Pos 2	3.41	5.16	32.06	59.37
Pos 3	3.77	5.06	32.12	59.06
Pos 4	3.76	4.96	32.38	58.90
Pos 5	3.77	5.04	32.54	58.65
Pos 6	4.09	5.30	31.15	59.46
Pos 7	3.75	4.87	32.56	58.81
Pos 8	5.05	4.89	30.70	59.35

X-ray Diffraction

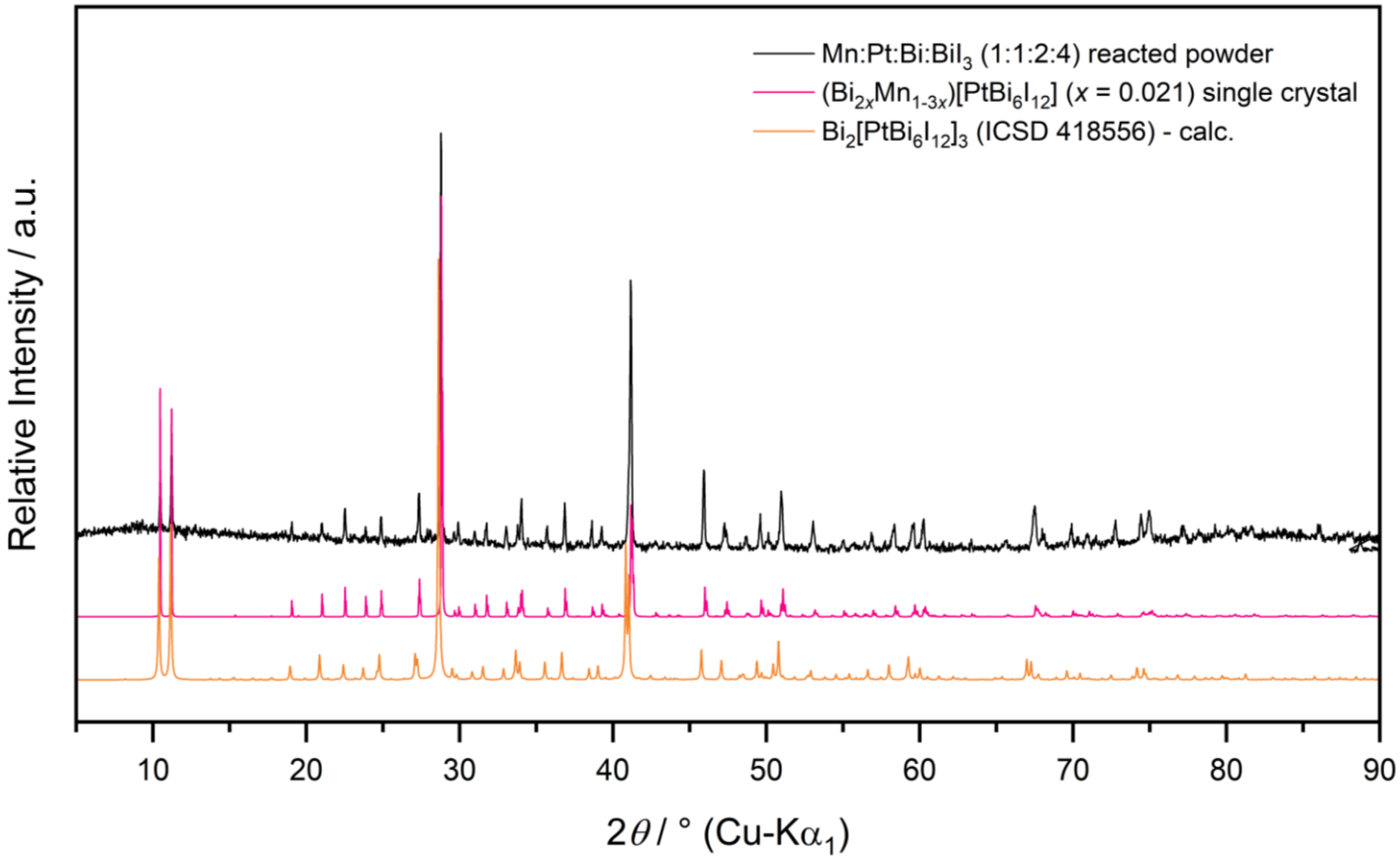

Figure S4. Representative powder X-ray diffractogram of a polycrystalline sample of $(Bi_{2x}Mn_{1-3x})[PtBi_6I_{12}]$ obtained by the synthesis protocol for powder samples (black). The reference patterns of $(Bi_{2x}Mn_{1-3x})[PtBi_6I_{12}]$ with $x \approx 0$ (magenta) and $Bi_{2/3}[PtBi_6I_{12}]$ (orange) were calculated from single-crystal data.

Table S3. Wyckoff position, coordinates, coefficients U_{ij} (/ pm^2) of the tensors of the anisotropic displacement factor, and equivalent displacement factor for the atoms in $(Bi_{2x}Mn_{1-3x})[PtBi_6I_{12}]$ with $x = 0.021(2)$ at 296(1) K. U_{eq} is defined as one third of the trace of the orthogonalized U_{ij} tensor. The Mn position is occupied with 93.6(5)% Mn and 4.3(3)% Bi.

Atom	W.p.	*x*	*y*	*z*	U_{11}	U_{22}	U_{33}	U_{23}	U_{13}	U_{12}	U_{eq}
Pt	3*a*	0	0	0	137.5(7)	137.5(7)	103(1)	0	0	68.8(3)	126.1(5)
Bi	18*f*	0.16391(2)	0.06474(2)	0.14593(2)	177.7(5)	275.5(6)	175.5(5)	–21.0(4)	–40.5(4)	112.7(5)	209.7(3)
Mn/Bi2	3*b*	0	0	½	300(5)	300(5)	161(6)	0	0	150(3)	254(4)
I1	18*f*	0.10885(2)	0.17793(2)	0.34811(2)	288(1)	235(1)	178.7(9)	–37.1(8)	–19.2(8)	115.8(9)	240.2(5)
I2	18*f*	0.29532(2)	0.24884(2)	–0.00838(3)	240(1)	393(1)	374(2)	129(1)	–102(1)	–26(1)	417.5(8)

Electrical Resistance Measurement

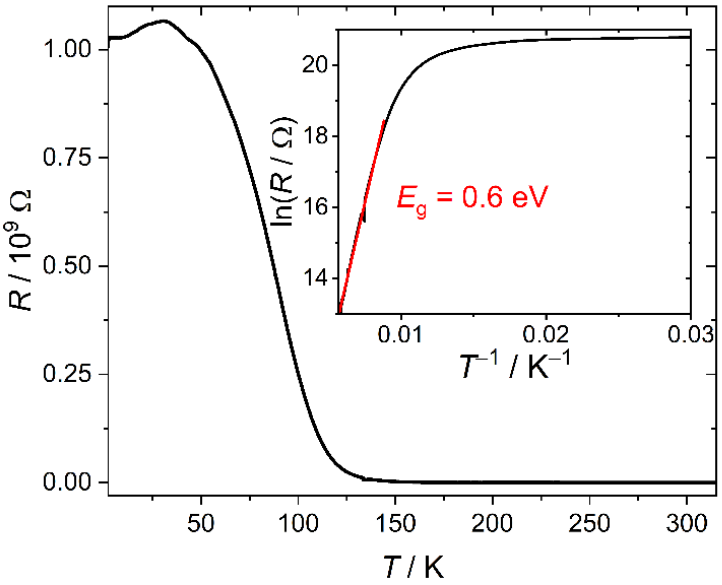

Figure S5. Temperature dependence of the electrical resistance of a Mn[$PtBi_6I_{12}$] powder sample. Inset: Arrhenius type plot and linear fit to the data between 110 and 170 K.

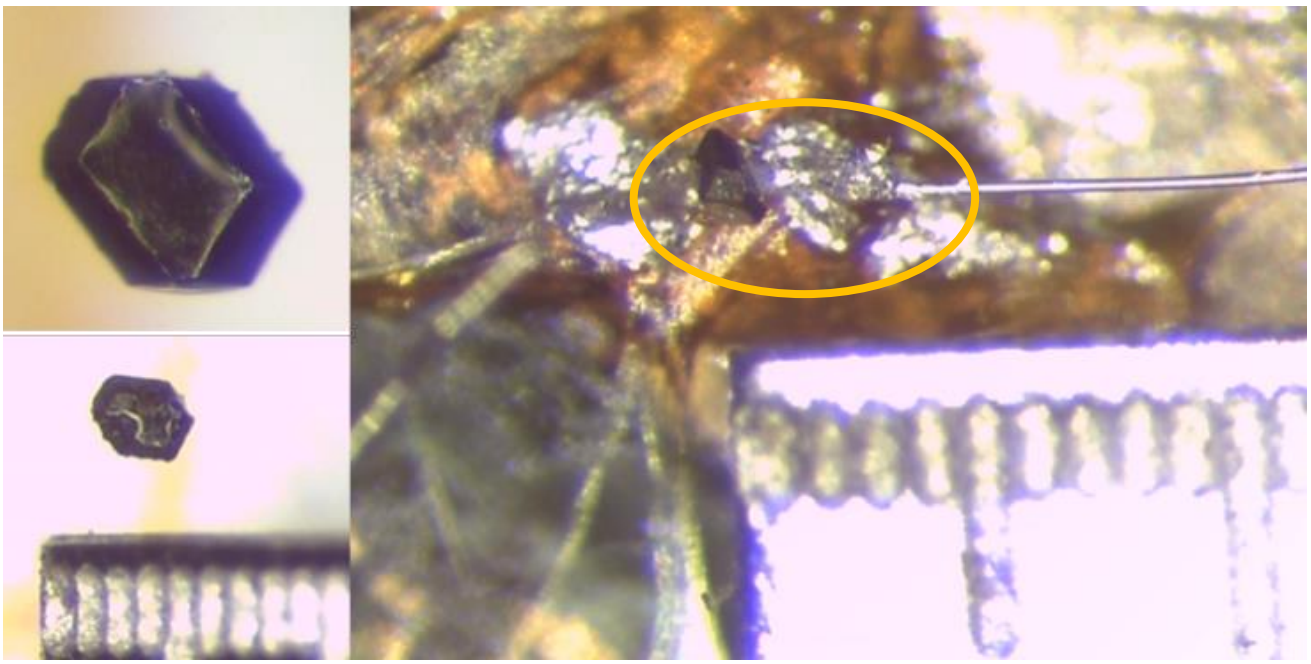

Figure S6. Left: Single-crystal of Mn[$PtBi_6I_{12}$] with the shape of a rhombic dodecahedron. One of the contacted facets is facing the viewer. Right: Crystal contacted by two Pt-wires using Ag epoxy. Small lines on ruler shown both on the left and right correspond to 0.1 mm divisions.

Magnetic Measurements

Table S4. Parameters determined from Curie-Weiss fits $\chi^{-1} = [\chi_0 + C/(T-\theta)]^{-1}$to the magnetic susceptibility data measured in external fields of 0.01 T ≤ $\mu_0 H$ ≤ 7 T and calculated effective magnetic moments per Mn atom.

$\mu_0 H$ /T	χ_0 / emu mol^{-1}	θ / K	C / emu K mol^{-1}	m_{eff}	m_{eff} per Mn
0.01	0.0017	–1.8	2.50	4.5 μ_B	5.7 μ_B
0.1	0.0015	–2.0	3.31	5.1 μ_B	6.5 μ_B
1	–0.00014	–1.3	3.29	5.1 μ_B	6.5 μ_B
3.5	–0.0006	–2.6	3.36	5.2 μ_B	6.6 μ_B
7	–0.0008	–4.6	3.43	5.2 μ_B	6.6 μ_B

Heat Capacity

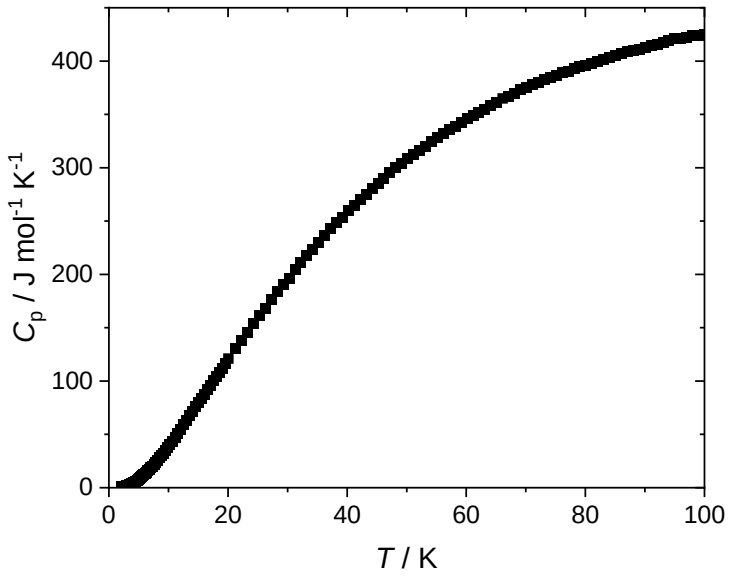

Figure S7. Specific heat capacity of a Mn[$PtBi_6I_{12}$] pressed powder sample.